Chemistry Europe
European Chemical Societies Publishing

Special Collection

A Chiral Molecular Cage Comprising Diethynylallenes and *N*-Heterotriangulenes for Enantioselective Recognition

Sandra Míguez-Lago,[a, b] Bettina D. Gliemann,[b] Milan Kivala,*[c, d] and María Magdalena Cid*[a]

In memory of Professor François Diederich

Abstract: Chirality, a characteristic tool of molecular recognition in nature, is often a complement of redox active systems. Scientists, in their eagerness to mimic such sophistication, have designed numerous chiral systems based on molecular entities with cavities, such as macrocycles and cages. In an attempt to combine chirality and redox-active species, in this contribution we report the synthesis and detailed characterization of a chiral shape-persistent molecular cage based on the combination of enantiopure diethynylallenes and electron-rich bridged triarylamines, also known as *N*-heterotriangulenes. Its ability for chiral recognition in solution was revealed through UV/vis titrations with enantiopure helicenes.

The rational design of artificial chiroptical sensors is essential given the chiral nature of the majority of biomolecules. Their scope encompasses applications ranging from molecular detection often related with medical diagnosis,[1] to the switching phenomenon in connection with molecular machines,[2] and chiral catalysis.[3] Such chiroptical sensors comprise a more or less open cavity, in which the higher the number of interactions between host and guest, the higher the specificity of the recognition event.[4] To this regard, 3D cage cavities are theoretically preferred over macrocyclic ones,[5] with size and shape being key factors to consider for an accurate chiral matching. Strategies to achieve chiral cages involve either the assembly of achiral units in a chiral fashion, often leading to statistic mixtures, or the direct use of enantiopure chiral building blocks.[6] Access to purely organic chiral molecular cages by the second approach has mostly emerged along with the research conducted on imine condensation starting from chiral amines by Mastalerz,[7] and Cooper and co-workers,[8] inter alia. Chemically stable axially chiral diethynylallenes (DEAs), initially employed in the synthesis of oligomers and macrocycles with intriguing chiroptical properties,[9,10] made also their foray into organometallic[11] and supramolecular chiral cages for the sensing of achiral guests by the Diederich group.[12] In its purely organic covalent variant, Cid and co-workers have demonstrated the feasibility of realizing chiral molecular cages with outstanding chiroptical properties from the combination of shape-persistent enantiopure DEAs and simple aromatic motifs for the detection of small achiral molecules (Figure 1, cages 1 and 2).[13–15] On this firm basis, we advocate the use of

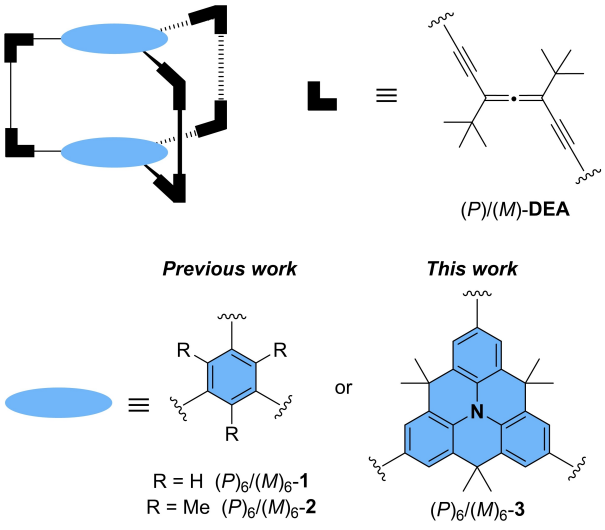

Figure 1. Schematic structures of the shape-persistent chiral molecular cages previously reported $(P)_6/(M)_6$-**1** and $(P)_6/(M)_6$-**2**, and the novel *N*-heterotriangulenic ones $(P)_6/(M)_6$-**3**.

[a] Dr. S. Míguez-Lago, Prof. M. M. Cid
Departamento de Química Orgánica
Universidade de Vigo
Campus Lagoas-Marcosende, 36310 Vigo (Spain)
E-mail: mcid@uvigo.es

[b] Dr. S. Míguez-Lago, Dr. B. D. Gliemann
Department of Chemistry and Pharmacy
Chair of Organic Chemistry I
Friedrich-Alexander-Universität Erlangen-Nürnberg
Nikolaus-Fiebiger-Str. 10, 91058 Erlangen (Germany)

[c] Prof. Dr. M. Kivala
Organisch-Chemisches Institut
Ruprecht-Karls-Universität Heidelberg
Im Neuenheimer Feld 270, 69120 Heidelberg (Germany)
E-mail: milan.kivala@oci.uni-heidelberg.de

[d] Prof. Dr. M. Kivala
Centre for Advanced Materials
Ruprecht-Karls-Universität Heidelberg
Im Neuenheimer Feld 225, 69120 Heidelberg (Germany)

Supporting information for this article is available on the WWW under https://doi.org/10.1002/chem.202101801

Special Collection This article belongs to a Joint Special Collection dedicated to François Diederich.

bridged triarylamines, known as *N*-heterotriangulenes (*N*-HTAs), in the role of chromophoric aromatic lids, in order to achieve redox-active nanosized cavities[16–20] for larger chiral guests, aiming at setting foot on the realm of enantioselective discrimination.[21–23]

Precedents of sensing examples involving triarylamines range from the detection of metallic cations,[24] to toxic anions[25] or anions present in chemical weapons,[26] nitroaromatic explosives,[27] biological metabolites,[28] toxic gases,[29,30] and pH determination.[31] Regarding the implementation of triarylamines in both macrocyclic and cage structures, few examples can be tracked down in literature,[32–39] and even scarcer examples are found for their bridged analogues, *N*-HTAs, whose presence in complexing and sensing processes is limited.[40–45] Besides exploring uncharted waters, *N*-HTA are also of interest given their solid candidacy for next-generation optoelectronic materials,[46–48] and properties such as reversible redox chemistry.[49]

Here we present the synthesis and full characterization of an organic covalent chiral cage composed of enantiopure DEAs and electron-rich dimethylmethylene-bridged *N*-HTAs together with the evidence for its enantioselective sensing ability in solution.

Triiodinated triangulene **4** was synthesized in 41% yield according to a previously reported procedure from the corresponding parent *N*-HTA **S1** (see the Supporting Information).[50] The chiral building block (*M*)-DEA was prepared in a five-step pathway, and both enantiomers resolved by chiral HPLC in the same way as in our previous reports.[13] Both the axially chiral (*M*)-DEA and the aromatic core **4** were connected affording the tripodal intermediate $(M)_3$-**5** in a 46% yield by a threefold Sonogashira cross-coupling between 1 equiv. of **4** and 3.3 equiv. of enantiopure (*M*)-DEA (Scheme 1, Figures S1–S3). Subsequent treatment of tripod-shaped molecule $(M)_3$-**5** with about 700 equiv. of flame-dried powdered NaOH in dry refluxing toluene for 1.5 h under N_2 yielded deprotected $(M)_3$-**6** in 49% yield (for characterization see Figures S4–S6 in the Supporting Information). Finally, compound $(M)_3$-**6** was added in dry pyridine under pseudo-high-dilution conditions ($\phi =$ 1 mL h^{-1}) to a solution of CuCl (75 equiv.) and $CuCl_2$ (11 equiv.) in dry pyridine under N_2 at room temperature for three days, affording $(M)_6$-**3** in a yield of 30% as a beige solid. The same synthetic procedure was applied to achieve enantiomer $(P)_6$-**3** with identical results. Compound $(M)_6$-**3** shows excellent solubility in different aprotic polar (CH_2Cl_2, $CHCl_3$, THF) and apolar (hexanes) organic solvents. The compound is configurationally stable towards racemization at ambient temperature and chemically stable under air atmosphere for months.

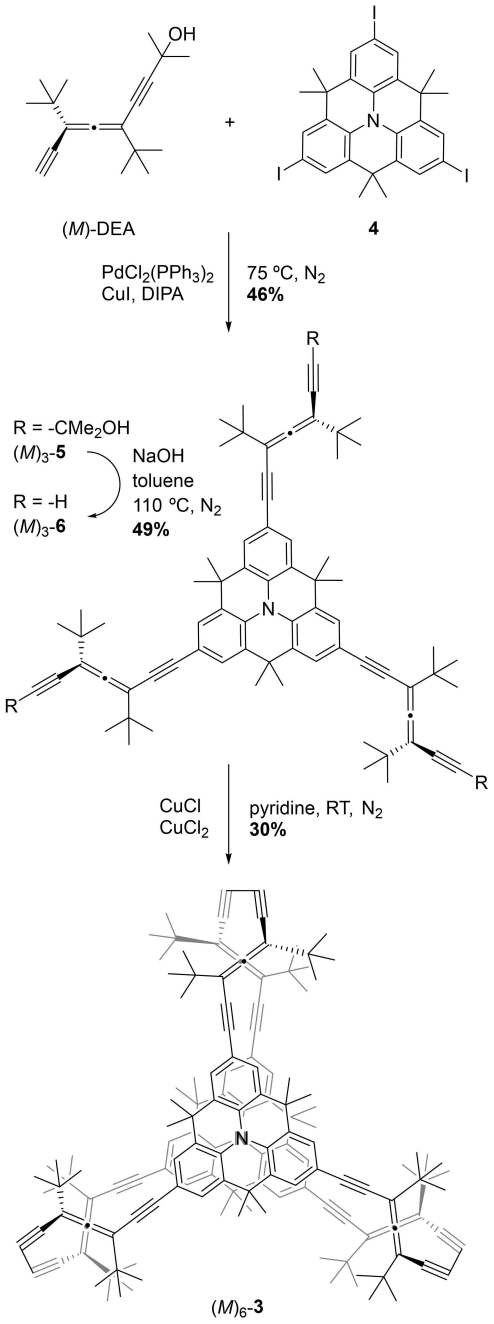

Scheme 1. Synthesis of chiral molecular cage $(M)_6$-**3**. An identical procedure was applied to the $(P)_6$ enantiomer giving comparable results. DIPA = *N*,*N*-diisopropylamine.

Both D_3 symmetric cage enantiomers $(M)_6$-**3** and $(P)_6$-**3** were fully characterized by means of ^{1}H, ^{13}C, HSQC and HMBC NMR, UV/vis and electronic circular dichroism (ECD) spectroscopies, and HR-MALDI mass spectrometry (Figures S7–S11). From the ^{1}H and ^{13}C NMR spectra of compound $(M)_6$-**3** a differentiating feature is deduced with respect to the previously reported benzenic molecular cage $(M)_6$-**1**, where the unsubstituted aromatic positions in *meta*- of the aromatic lids were chemically equivalent. In $(M)_6$-**3**, however, these free aromatic *meta*-positions are diastereotopic, producing splitting in two ^{1}H signals at 7.33 and 7.30 ppm (Figure 2) and six different ^{13}C signals at 131.4, 130.1, 130.0, 126.8, 126.6, and 118.3 ppm. Furthermore, the bridging methyl groups show different chemical shifts at 1.66 and 1.37 ppm, most likely corresponding to the ones pointing outward and inward the cage cavity, respectively (Figure 2), given the shielding cone effect inside the cage. This peculiar property allows the NMR determination of the relative positions of host and guest throughout the binding process, even in the absence of an X-ray crystal

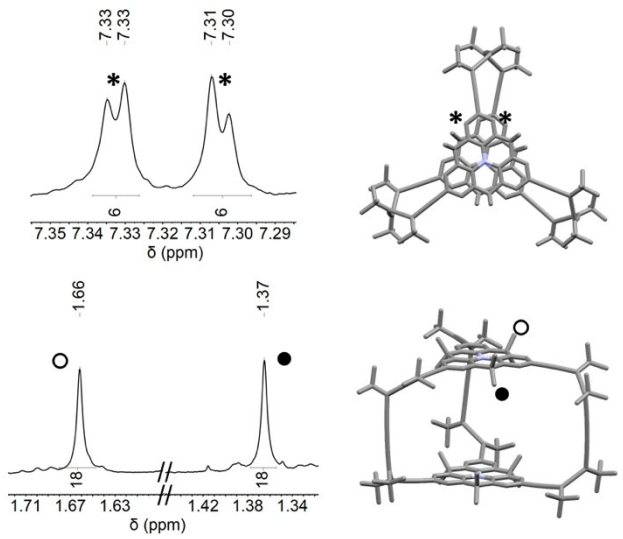

Figure 2. ^{1}H NMR spectrum cuts of $(M)_6$-**3** in $CDCl_3$ (400 MHz). Tentative signal assignment and top and lateral views of the optimized structure of $(M)_6$-**3** at the B3LYP/6-31G level of theory.

structure of the complex, according to the degree of chemical shift experienced by the signals. HSQC and HMBC ^{1}H,^{13}C single and multiple-bond correlations were assigned in $CDCl_3$ (Figures S9 and S10).

UV/vis spectroscopy measurements of target compound $(M)_6$-3 were conducted in $CHCl_3$, being the molar absorptivity $\varepsilon = 108000\ m^{-1}\,cm^{-1}$ at the maximum absorption wavelength 378 nm and the maximum dissymmetry factor equal to 0.007 at 306 nm, which indicates a high degree of chiral amplification and chiroptical discrimination power compared to our previous reports.[13] Electronic circular dichroism (ECD) spectrum of $(M)_6$-**3** in $CHCl_3$ shows a very intense positive band at about 260 nm, along with a pronounced shoulder-containing negative band at about 300 nm, followed by weaker alternating positive and negative Cotton effects with maxima at about 370 and 400 nm, respectively (Figure 3). The ECD spectrum of $(P)_6$-**3** is a perfect mirror image of its enantiomer $(M)_6$-**3**.

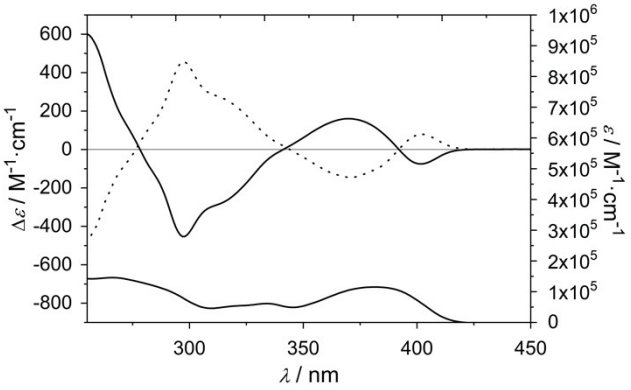

Figure 3. UV/vis absorption and ECD spectra of $(M)_6$-**3** (solid line) and $(P)_6$-**3** (dotted line) in $CHCl_3$.

To assess the redox properties of molecular cage $(M)_6$-**3** cyclic voltammetry measurements in CH_2Cl_2 were conducted. We observe two reversible oxidation waves at +0.41 and +0.44 V (vs. ferrocene/ferrocenium (Fc/Fc^+)), respectively, which can be attributed to the formation of the double radical cationic species (Figure S12).[49] In comparison to parent unsubstituted *N*-HTA (**S1**), with an oxidation wave centered at +0.34 V, an anodic shift in cage $(M)_6$-**3** appears as a result from the moderate EWG effect of the DEA units. These finding holds considerable promise for this system to be employed as a potential redox sensing agent.

In comparison with its mesitylene analogue $(M)_6$-**2** chiral molecular cage $(M)_6$-**3** features more electron-rich aromatic lids due to the delocalized amine lone pair over the polycyclic framework (see Figure S16 for the corresponding electrostatic potential map). Furthermore, the cage possesses a larger cavity with an estimated volume of 2040 Å^3 (approximated cylindrical cavity height and diameter = 9.03 and 17.76 Å, respectively; Figure S15). In addition, the *N*-HTA lids in $(M)_6$-**3** endow the chiral cage with the possibility of not only establishing the C–H···π and π···π interactions with the potential guest, but also additional hydrophobic contacts provided by their inward-pointing methyl group of the dimethylmethylene bridges. To establish a solid starting point on the evaluation of complexation ability of $(M)_6$-**3**, studies comparing complex formation between molecular cages $(M)_6$-**1**, $(M)_6$-**2**, and current $(M)_6$-**3** with η^5-cyclopentadienyl-η^6-naphthaleneruthenium(III) hexafluorophosphate (Figure S19, Rut^+) sandwich compound as a guest were performed. Analysis of the titrations resulted in a $Rut^+@(M)_6$-**3** association constant of $590 \pm 65\ M^{-1}$ for the 1:1 complex. This value entails one half of the previously achieved for complex $Rut^+@(M)_6$-**2** ($905\ M^{-1}$ for the 1:1 complex), fact which concurs with a lower packing coefficient (P.C.) given the bigger cavity volume for host **3**. With regards to complex $Rut^+@(M)_6$-**1** ($50\ M^{-1}$ for the 1:1 complex), the new molecular cage $(M)_6$-**3** gave rise to an almost 12-fold association constant, reflecting the richer electronic character of the triangulenic lids (for more details see the Supporting Information, Figures S17–S19).

In view of the positive results achieved for $(M)_6$-**3** in complex formation with Rut^+, we directed our efforts to enantioselective molecular recognition processes, envisioning chirality as a benefit for the host-guest match. For this purpose, helical guest (Hel; Figure 4a) was proposed for the complexation with our chiral cage $(M)_6$-**3**. Sulfone-bridged hetero[4]helicene Hel was synthesized from its parent dithia-bridged *N*-heterohelicene,[51] through oxidation with a 1:1 *v/v* mixture of glacial acetic acid and H_2O_2 (30% *w/w* in H_2O) at 120 °C in a 93% yield (Figures S13 and S14).

Thus, titrations at constant concentration of host $(M)_6/(P)_6$-**3** with chiral guest (*P*)/(*M*)-Hel were performed by means of UV/vis spectroscopy in $CHCl_3$ (Figures S20 and S21) with data treatment employing the *BindFit* v0.5 online software package,[52] with a 1:1 global fitting model (Nelder-Mead method).[53] Up to three titrations were done for each of both homochiral and heterochiral combinations. Saturation curves for the four possible guest@host diastereomeric complexes

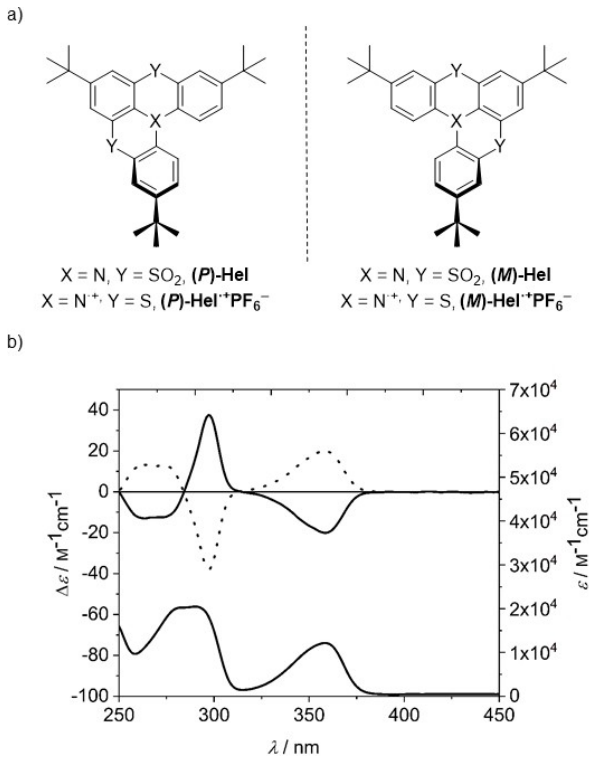

Figure 4. a) Helicene enantiomers of Hel and Hel$^{\bullet+}$ (PF_6^- as counterion). b) ECD (top) and UV/vis (bottom) spectra of Hel enantiomers in $CHCl_3$. Dotted line (*M*)-**Hel**, solid line (*P*)-**Hel**.

were evaluated at 325 nm ($\varepsilon_{HOST} \approx 10^5\ M^{-1}cm^{-1}$, $\varepsilon_{GUEST} \approx 10^3\ M^{-1}cm^{-1}$) for up to 300 equiv. of the guest (Figure S22), with the corresponding linear fittings of the Benesi-Hildebrand plots having good coefficients of determination ($R^2 = 0.9919$–0.9996; Figure S23).

As a result, association constants for the two diastereomeric complexes (two enantiomeric homochiral *P@P* and *M@M*, and two enantiomeric heterochiral *P@M* and *M@P*) were calculated (Table 1). The mean value thereof is of the same magnitude as for Rut$^+$@3, despite the electrostatic component being less favored for neutral species Hel, most likely compensated by the larger guest volume ($V_{Hel} = 375$ Å^3 calculated using *Spartan'08*) which results in a packing coefficient of 18%. Regarding the chiral discrimination, there is a preference for the heterochiral

Table 1. Association constants calculated for the 1:1 Hel@**3**, and for the 1:1 and 2:1 Hel$^{\bullet+}$@**3** diastereomeric complexes in $CHCl_3$.

	K_{11} [M^{-1}]		K_{11} and K_{12} [M^{-1}][b]	
	(*Y*)-Hel	(*X*)-Hel	(*Y*)-Hel$^{\bullet+}$	(*X*)-Hel$^{\bullet+}$
(*X*)$_6$-**3**	246 ± 81 363 ± 104[a]	172 ± 42 97 ± 10[a]	42725 ± 13255 303 ± 48	64585 ± 28430 306 ± 88

Standard deviation from both homochiral and heterochiral enantiomeric combinations. (*X*) and (*Y*) stand for generic chirality absolute configuration descriptors (*M*) or (*P*) indistinctly. [a] Values obtained via ECD titrations in $CHCl_3$ at 325 nm. [b] K_{11} (larger values) and K_{12} (smaller values) describe the formation of guest@host 1:1 and 2:1 complexes respectively.

complex formation observed by means of UV/vis titrations (K_a-heterochiral/K_a-homochiral ≈ 1.4), corroborated as well by the ECD analysis (K_a-heterochiral/K_a-homochiral ≈ 3.7). These values hint at a different stability of the diastereomeric complexes.[54] Therefore, in order to gain insight into the binding in terms of intermolecular host-guest interactions, optimization and frequencies at the B3LYP/6-31G level of theory in the gas phase were calculated for the four possible Hel@3 diastereomeric complexes. The optimized structures show S=O···H contact distances, with oxygen atoms belonging to guest Hel and hydrogen atoms from the triangulene dimethylmethylene bridges, ranging from 2.3 to 2.9 Å and π···π interactions with distances between 4.5 and 4.7 Å (Figures 5 and S26), which points to synergistic interactions as main driving force of the complexation with a certain degree of parallel-displaced π···π contribution, beyond the classically accepted limits within π···π interactions.[55] Despite DFT calculations at the B3LYP/6-31G arose no significant energy differences between the diastereomeric complexes (up to 0.06 kcal mol^{-1}), small differences in the array of weak interactions between host and guest account for the degree of enantioselectivity found, as previously reported in literature for different substrate-receptor complexes.[56]

To further enhance the association constants, the possibility of including stronger interactions such as cation···π was exploited. Thus, previously reported radical cation Hel$^{\bullet+}$ (Figure 4a)[51] was examined as a guest with molecular cages (*P*)$_6$/(*M*)$_6$-3 by means of UV/vis titrations (Figures S24 and S25), following the same aforementioned data treatment. In this case, data fitting evidenced the formation of 2:1 complexes, whose K_{11} values for the two possible guest@host diastereomeric combinations show a substantial increase between 2 and 3 orders of magnitude with respect to the neutral helicene Hel (Table 1). Curiously, in this case a preference is observed for the formation of homochiral complexes (*P*)-Hel$^{\bullet+}$@(*P*)$_6$-**3** and (*M*)-Hel$^{\bullet+}$@(*M*)$_6$-**3**, with a K_a homochiral/heterochiral ratio of about 1.5. This values point to a similar enantioselectivity to that of complexation involving sulfone-bridged helicene Hel.[57] As further evidence of the complex formation with guest Hel$^{\bullet+}$, ESI HRMS measurements showed ion peaks corresponding to the [1:1]$^+$ and [2:1]$^+$ complexes at the theoretical 2387.4508 and

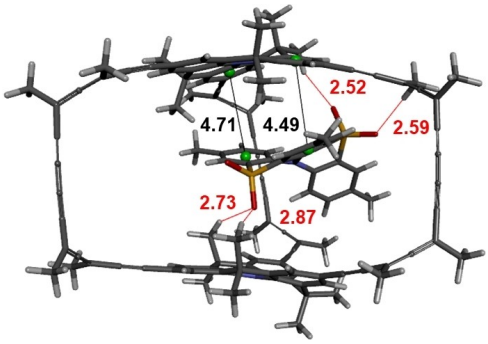

Figure 5. Computed structure of complex (*M*)-Hel@(*P*$_6$)-**3** at B3LYP/6-31G level of calculation with labeled S=O···H contacts (red), and π···π interactions (black). Distances in Å.

2862.6744 mass/charge ratios for the four diastereomeric combinations (Figures S27–S40).

In conclusion, novel D_3 symmetric chiral cages $(P)_6/(M)_6$-**3**, which combine redox-active *N*-heterotriangulenes and enantiopure diethynylallenes, were synthesized in good yield and fully characterized by means of NMR, IR, UV/vis and ECD spectroscopies as well as mass spectrometry. Moreover, their ability as chiral host was demonstrated by complexation experiments with chiral guests Hel and Hel$^{\bullet+}$, which were conducted by UV/vis titration pointing at a certain degree of enantioselectivity. For Hel K_a heterochiral/homochiral ratios of 1.4 and 3.7 by means of UV/vis and ECD were obtained, respectively, whereas for Hel$^{\bullet+}$ a K_a homochiral/heterochiral ratio of 1.5 was obtained, with homochiral complexes being the favored ones. Hence, this report constitutes the first example of a chiral host bearing a large and shape-persistent cavity, merging *N*-heterotriangulene lids and diethynylallene-based branches providing the chiral discrimination feature. The development of receptors of this kind envisions future applications in the selective sensing of redox-active chiral species with dual modulation grounded on both their chiral configuration and oxidation degree.

Acknowledgements

S.M.L. thanks the Marie Curie Action "International Network on Integrated Techniques in Structural Elucidation" (INTechSE) and the FAU Erlangen-Nürnberg for the funding provided by the FFL postdoctoral program and the Emerging Talents Initiative (ETI 2018/1_Nat_02) grant. M.M.C. thanks financial support from Ministerio de Economia y Competitividad of Spain (CTQ2017-85919-R). M.K. acknowledges generous funding by the Deutsche Forschungsgemeinschaft (DFG) – projects no. 182849149-SFB 953 and 281029004-SFB 1249.

Conflict of Interest

The authors declare no conflict of interest.

Keywords: allenes · bridged triarylamines · chirality · molecular cages · molecular recognition

[1] L. Tang, S. Li, L. Xu, W. Ma, H. Kuang, L. Wang, C. Xu, *ACS Appl. Mater. Interfaces* **2015**, *7*, 12708–12712.
[2] S. Kassem, A. T. L. Lee, D. A. Leigh, V. Marcos, L. I. Palmer, S. Pisano, *Nature* **2017**, *549*, 374–378.
[3] Y. Wang, Y. Sun, P. Shi, M. M. Sartin, X. Lin, P. Zhang, H. Fang, P. Peng, Z. Tian, X. Cao, *Chem. Sci.* **2019**, *10*, 8076–8082.
[4] A. Berthod, *Anal. Chem.* **2006**, *78*, 2093–2099.
[5] K. Kajiyama, E. Tsurumaki, K. Wakamatsu, G. Fukuhara, S. Toyota, *ChemPlusChem* **2021**, *86*, 716–722.
[6] A. Ozcelik, R. Pereira-Cameselle, N. P. Ulrih, A. G. Petrovic, J. L. Alonso-Gómez, *Sensors* **2020**, *20*, 974–996.
[7] M. Mastalerz, *Acc. Chem. Res.* **2018**, *51*, 2411–2422.
[8] M. E. Briggs, A. I. Cooper, *Chem. Mater.* **2017**, *29*, 149–157.
[9] S. Odermatt, J. L. Alonso-Gómez, P. Seiler, M. M. Cid, F. Diederich, *Angew. Chem. Int. Ed.* **2005**, *44*, 5074–5078; *Angew. Chem.* **2005**, *117*, 5203–5207.
[10] P. Rivera-Fuentes, J. L. Alonso-Gómez, A. G. Petrovic, F. Santoro, N. Harada, N. Berova, F. Diederich, *Angew. Chem. Int. Ed.* **2010**, *49*, 2247–2250; *Angew. Chem.* **2010**, *122*, 2296–2300.
[11] O. Gidron, M.-O. Ebert, N. Trapp, F. Diederich, *Angew. Chem. Int. Ed.* **2014**, *53*, 13614–13618; *Angew. Chem.* **2014**, *126*, 13833–13837.
[12] C. Gropp, N. Trapp, F. Diederich, *Angew. Chem. Int. Ed.* **2016**, *55*, 14444–14449; *Angew. Chem.* **2016**, *128*, 14659–14664.
[13] S. Míguez-Lago, A. L. Llamas-Saiz, M. Magdalena Cid, J. L. Alonso-Gómez, *Chem. Eur. J.* **2015**, *21*, 18085–18088.
[14] S. Míguez-Lago, M. M. Cid Fernández, J. L. Alonso Gómez, *Eur. J. Org. Chem.* **2016**, *2016*, 5716–5721.
[15] S. Míguez-Lago, M. M. Cid, *Synthesis* **2017**, *49*, 4111–4123.
[16] T. A. Barendt, W. K. Myers, S. P. Cornes, M. A. Lebedeva, K. Porfyrakis, I. Marques, V. Félix, P. D. Beer, *J. Am. Chem. Soc.* **2020**, *142*, 349–364.
[17] G. Li, T. Matsuno, Y. Han, H. Phan, S. Wu, Q. Jiang, Y. Zou, H. Isobe, J. Wu, *Angew. Chem. Int. Ed.* **2020**, *59*, 9727–9735; *Angew. Chem.* **2020**, *132*, 9814–9822.
[18] P. Ribar, T. Šolomek, M. Juríček, *Org. Lett.* **2019**, *21*, 7124–7128.
[19] W. Liu, S. Bobbala, C. L. Stern, J. E. Hornick, Y. Liu, A. E. Enciso, E. A. Scott, J. Fraser Stoddart, *J. Am. Chem. Soc.* **2020**, *142*, 3165–3173.
[20] Y. Ni, F. Gordillo-Gámez, M. Peña Alvarez, Z. Nan, Z. Li, S. Wu, Y. Han, J. Casado, J. Wu, *J. Am. Chem. Soc.* **2020**, *142*, 12730–12742.
[21] A. U. Malik, F. Gan, C. Shen, N. Yu, R. Wang, J. Crassous, M. Shu, H. Qiu, *J. Am. Chem. Soc.* **2018**, *140*, 2769–2772.
[22] T. R. Schulte, J. J. Holstein, G. H. Clever, *Angew. Chem. Int. Ed.* **2019**, *58*, 5562–5566; *Angew. Chem.* **2019**, *131*, 5618–5622.
[23] R. J. Pieters, J. Cuntze, M. Bonnet, F. Diederich, *J. Chem. Soc. Perkin Trans. 2* **1997**, *28*, 1891–1900.
[24] P. Thamaraiselvi, N. Duraipandy, M. S. Kiran, S. Easwaramoorthi, *ACS Sustainable Chem. Eng.* **2019**, *7*, 9865–9874.
[25] P. B. Pati, S. S. Zade, *Eur. J. Org. Chem.* **2012**, *2012*, 6555–6561.
[26] M. Steeger, C. Lambert, *Chem. Eur. J.* **2012**, *18*, 11937–11948.
[27] X. Zhang, Q. Lu, C. Yang, S. Zhao, Y. Wang, W. Zhang, H. Niu, P. Zhao, W. Wang, J. Fan, *New J. Chem.* **2019**, *43*, 1177–1185.
[28] T. Jiang, N. Lu, Y. Hang, J. Yang, J. Mei, J. Wang, J. Hua, H. Tian, *J. Mater. Chem. C* **2016**, *4*, 10040–10046.
[29] Z. Ning, Z. Chen, Q. Zhang, Y. Yan, S. Qian, Y. Cao, H. Tian, *Adv. Funct. Mater.* **2007**, *17*, 3799–3807.
[30] A. Das, R. Dost, T. Richardson, M. Grell, J. J. Morrison, M. L. Turner, *Adv. Mater.* **2007**, *19*, 4018–4023.
[31] B. Hu, X. Chen, Y. Wang, P. Lu, Y. Wang, *Chem. Asian J.* **2013**, *8*, 1144–1151.
[32] H. Itoi, T. Jang, S. Kanehashi, T. Shimomura, K. Ogino, *Tetrahedron Lett.* **2017**, *58*, 3579–3582.
[33] Q. Kong, H. Qian, Y. Zhou, J. Li, H. Xiao, *Mater. Chem. Phys.* **2012**, *135*, 1048–1056.
[34] J.-H. Tang, Y. Sun, Z.-L. Gong, Z.-Y. Li, Z. Zhou, H. Wang, X. Li, M. L. Saha, Y.-W. Zhong, P. J. Stang, *J. Am. Chem. Soc.* **2018**, *140*, 7723–7729.
[35] X. F. Yang, M. Liu, H. Bin Zhu, *Inorg. Chem. Commun.* **2017**, *83*, 40–43.
[36] B. Mondal, K. Acharyya, P. Howlader, P. S. Mukherjee, *J. Am. Chem. Soc.* **2016**, *138*, 1709–1716.
[37] F. A. Neugebauer, S. Kuhnhäuser, *Angew. Chem. Int. Ed.* **1985**, *24*, 596–597; *Angew. Chem.* **1985**, *97*, 589–590.
[38] Y. Yokoyama, D. Sakamaki, A. Ito, K. Tanaka, M. Shiro, *Angew. Chem. Int. Ed.* **2012**, *51*, 9403–9406; *Angew. Chem.* **2012**, *124*, 9537–9540.
[39] S. Sathyamoorthi, J. T. Mague, R. A. Pascal, *Org. Lett.* **2012**, *14*, 3427–3429.
[40] F. Schlütter, F. Rossel, M. Kivala, V. Enkelmann, J.-P. Gisselbrecht, P. Ruffieux, R. Fasel, K. Müllen, *J. Am. Chem. Soc.* **2013**, *135*, 4550–4557.
[41] K. Cui, F. Schlütter, O. Ivasenko, M. Kivala, M. G. Schwab, S.-L. Lee, S. F. L. Mertens, K. Tahara, Y. Tobe, K. Müllen, K. S. Mali, S. De Feyter, *Chem. Eur. J.* **2015**, *21*, 1652–1659.
[42] C. G. Frankær, T. J. Sørensen, *ACS Omega* **2019**, *4*, 8381–8389.
[43] C. G. Frankær, M. Rosenberg, M. Santella, K. J. Hussain, B. W. Laursen, T. J. Sørensen, *ACS Sens.* **2019**, *4*, 764–773.
[44] B. Qiao, B. E. Hirsch, S. Lee, M. Pink, C.-H. Chen, B. W. Laursen, A. H. Flood, *J. Am. Chem. Soc.* **2017**, *139*, 6226–6233.
[45] B. D. Gliemann, V. Strauss, J. F. Hitzenberger, P. O. Dral, F. Hampel, J.-P. Gisselbrecht, T. Drewello, W. Thiel, D. M. Guldi, M. Kivala, *Chem. Eur. J.* **2017**, *23*, 12353–12362.
[46] M. Hirai, N. Tanaka, M. Sakai, S. Yamaguchi, *Chem. Rev.* **2019**, *119*, 8291–8331.
[47] T. A. Schaub, K. Padberg, M. Kivala, *J. Phys. Org. Chem.* **2020**, *33*, e4022.
[48] M. Krug, M. Wagner, T. A. Schaub, W. Zhang, C. M. Schüßlbauer, J. D. R. Ascherl, P. W. Münich, R. R. Schröder, F. Gröhn, P. O. Dral, M. Barbatti,

D. M. Guldi, M. Kivala, *Angew. Chem. Int. Ed.* **2020**, *59*, 16233–16240; *Angew. Chem.* **2020**, *132*, 16368–16376.
[49] M. Krug, N. Fröhlich, D. Fehn, A. Vogel, F. Rominger, K. Meyer, T. Clark, M. Kivala, D. M. Guldi, *Angew. Chem. Int. Ed.* **2021**, *60*, 6771–6777; *Angew. Chem.* **2021**, *133*, 6845–6851.
[50] Z. Fang, T.-L. Teo, L. Cai, Y.-H. Lai, A. Samoc, M. Samoc, *Org. Lett.* **2009**, *11*, 1–4.
[51] B. D. Gliemann, A. G. Petrovic, E. M. Zolnhofer, P. O. Dral, F. Hampel, G. Breitenbruch, P. Schulze, V. Raghavan, K. Meyer, P. L. Polavarapu, N. Berova, M. Kivala, *Chem. Asian J.* **2017**, *12*, 31–35.
[52] http://supramolecular.org/.
[53] P. Thordarson, *Chem. Soc. Rev.* **2011**, *40*, 1305–1323.
[54] In this case, ^{1}H NMR titrations in $CDCl_3$ could not be analyzed due to overlapping between host and guest signals throughout both aromatic and dimethylmethylenic regions on the spectra, whilst the shift observed for *t*Bu groups in **3** is below the technique error.
[55] R. Kruszynski, T. Sierański, *Cryst. Growth Des.* **2016**, *16*, 587–595.
[56] R. Carrillo, M. López-Rodríguez, V. S. Martín, T. Martín, *Angew. Chem. Int. Ed.* **2009**, *48*, 7803–7808; *Angew. Chem.* **2009**, *121*, 7943–7948.
[57] Similar complexation tests through ^{1}H NMR titrations could not be performed given the paramagnetic character of $HeI^{\bullet+}$, which broadens the signals on the spectra.

Manuscript received: May 21, 2021
Version of record online: August 12, 2021

